Density-functional calculations and eigenchannel analyses for electron transport in Al and Si atomic wires

Shinya Okano,[1,2] Kenji Shiraishi,[1,3] and Atsushi Oshiyama[1,3]
[1]*Institute of Physics, University of Tsukuba, 1-1-1 Tennodai, Tsukuba 305-8571, Japan*
[2]*Research and Development for Applying Advanced Computational Science and Technology (ACT-JST), Japan Science and Technology Corporation, Kawaguchi, Saitama 332-0012, Japan*
[3]*Research Consortium for Synthetic Nano-Function Materials Project (SYNAF), National Institute of Advanced Industrial Science and Technology (AIST), 1-1-1 Umezono, Tsukuba 305-8568, Japan*
(Received 14 August 2003; published 7 January 2004)

We perform first-principles calculations of the conductance of Al and Si atomic wires between jellium electrodes using the wave-function matching method combined with the density-functional theory. The calculated conductances for single-line and double-line atomic wires exhibit rich variation depending on the detailed atomic structure and the chemical difference between the constituent elements. The origin of the similarity and dissimilarity between Al and Si atomic wires is unequivocally clarified by our eigenchannel analyses of the wave functions and transmission probabilities obtained and by the calculated energy bands of the corresponding infinite-length atomic wires. We also find that the conductance of single-line Al wires increases upon stretching of the wires. This is due to peculiar features of the electron states of atomic wires consisting of group III or group IV atoms. The result is consistent with the observed conductance of Al wires.

DOI: 10.1103/PhysRevB.69.045401 PACS number(s): 73.63.Rt, 73.40.Jn

I. INTRODUCTION

Recent developments in fabrication techniques such as the scanning tunneling microscope (STM) and the mechanically controllable breaking junction (MCBJ) enable us to form nanoscale metal contacts. Electron transport measurements have been carried out for such contacts and ballistic transport behaviors are usually observed.[1] In those experiments, structural variations during the conductance measurement usually take place and an interesting relationship between the atomic-scale structure and the electron conductance has been discovered.

A contact made of gold offers such an example. Ohnishi *et al.*[2] formed a nanoscale gold bridge by putting a gold STM tip on the Au surface and then withdrawing the tip. They observed Au bridges consisting of a few atom lines using the transmission electron microscope (TEM). The TEM clarified that the bridge becomes thinner line by line upon withdrawal. Moreover, simultaneous measurement of the electron conductance shows clear quantization of the conductance in units of $G_0=2e^2/h$ and a one-to-one correspondence between the value of the conductance and the thickness of the nanobridge. The conductance of the thinnest bridge is shown to be G_0, which implies ballistic transport in a single channel.

Aluminum nanocontacts exhibit different characteristics. Quantization of the conductance has indeed been observed in contacts fabricated using the STM and the MCBJ technique:[3–7] The conductance $G=\alpha G_0$ shows a steplike decrease with increasing electrode distance from the contact. In contrast to the gold contacts, however, α is close but not exactly equal to an integer. More surprisingly, α *increases* on each plateau of the conductance with increasing electrode distance. The number of transmitting channels has also been evaluated experimentally by using superconducting contacts:[5,7] It is shown that more than two channels contribute to the transport even when G is equal to $\sim G_0$, and a possible relation to the number of valence orbitals is speculated.[7]

Nanocontacts made of other metallic elements also exhibit the quantization of conductance and, moreover, element-dependent characteristics in the behavior of the conductance associated with structural changes.[3,6,7]

As for theory, there are several conductance calculations for Al wires based on density-functional theory (DFT).[8–11] Kobayashi *et al.* performed conductance calculations for a three-atom Al wire by the recursion-transfer matrix method. Their eigenchannel decomposition[12,13] shows that the number of relevant channels of a three-atom wire is three.[9,13,14] They also proposed that the change from the bent to the straight structure causes a positive slope of the conductance on each plateau. From a tight-binding calculation for a one-atom Al contact, Cuevas *et al.* found that the number of channels is three.[6] They also argued that the positive slope is due to the change of electron states caused by bond elongation, which contradicts the results by Kobayashi *et al.* Further investigation is certainly required to clarify the origin of the positive slope on each plateau of the conductance with elongating nanocontacts.

Those experimentally observed characteristics imply a wealth of underlying physics in nanoscale contacts. What is the relationship among nanoscale atomic structures, electron states, and quantum conductance? What is the role of differences in chemical elements in the conductance? In spite of extensive effort, a satisfactory understanding of those issues is still missing.

In order to clarify these interesting aspects of the relationship between the conductance and atomic structures or the conductance and chemical species, we here carry out conductance calculations within the density-functional scheme for prototype atomic wires consisting of Al and Si. We focus on salient features of the conductance of the atomic wires so

that geometry optimization of the structures is not pursued here. Instead, we choose several ideal atomic wires and then clarify the effects of the atomic geometry on the conductance. It is found that two neighboring elements in the periodic table exhibit quite different characteristics in the conductance when they are formed into nanostructures. We found that this difference can be well understood in terms of the electronic structures of atomic wires. In particular, the origin of the exotic and surprising behaviors of Al nanowires during elongation is naturally explained by the present calculation.

In Sec. II, we briefly explain our calculational methods. Results for single-line atomic wires are presented in Sec. III A, and the increase in the conductance of the Al nanowires is explained in Sec. III B. Characteristics of the double-line atomic wires are presented in Sec. III C. Section IV concludes the paper.

II. COMPUTATIONAL METHODS

Calculations are performed using density-functional theory[15,16] in describing interactions among electrons and using the multichannel Landauer formula[17] in obtaining the conductance. The transmission probability of an electron with a certain energy is computed by the wave-function matching (WFM) method.[18]

We consider the conductance of Al and Si atomic wires between two semi-infinite jellium electrodes at the zero-bias-voltage limit. The jellium is specified by the parameter $r_s = 2$ a.u., which corresponds to the electron density of bulk Al. Nuclei and core electrons for each atom constituting the atomic wires are represented by local pseudopotentials parametrized for Al (Ref. 19) and Si.[20] Interactions among valence electrons are treated in the local density approximation (LDA).[21,22] The distance between the end atom of the wire and the jellium edge is set to be 2.6 a.u. and 2.3 a.u. for Al and Si wires, respectively. These values are adopted from calculations for the stable geometries of adsorbed Al and Si atoms on a jellium surface.[23,24]

First we calculate the self-consistent potential $V(\boldsymbol{r})$ for an electron which is injected from the left electrode, passes through the atomic wire, and then reaches the right electrode. For that purpose, we divide the electrode-wire-electrode system into three regions: the left electrode, the right electrode, and the wire regions. For each region, self-consistent DFT-LDA calculations are performed. In these calculations we use a three-dimensional supercell model in which the wire or the electrode is placed in a large unit cell and periodic boundary conditions are imposed in three directions both parallel (z) and perpendicular (x and y) to the wire (Fig. 1). To simulate a single isolated wire, we take the large dimension 20 a.u. in the x and y directions. The self-consistent potential obtained in this supercell model is later used to calculate incident, reflected, and transmitted electron waves in the semi-infinite electrodes plus the finite-length atom wire. Therefore the ''wire region'' should contain substantially thick electrodes connected with both end atoms of the wire. This procedure enables us to describe potential modification near electrode-wire interfaces and to connect the ''wire region'' to the ''electrode'' regions smoothly. We find that an electrode with the thickness of 13 a.u. at both sides of the wire in the ''wire region'' is sufficient for the procedure. The Kohn-Sham orbitals and thus the electron density are expanded using a plane-wave basis set with cutoff energy of 4.0 Ry and 6.0 Ry for Al and Si, respectively. The Brillouin zone integration is done by Γ point sampling.

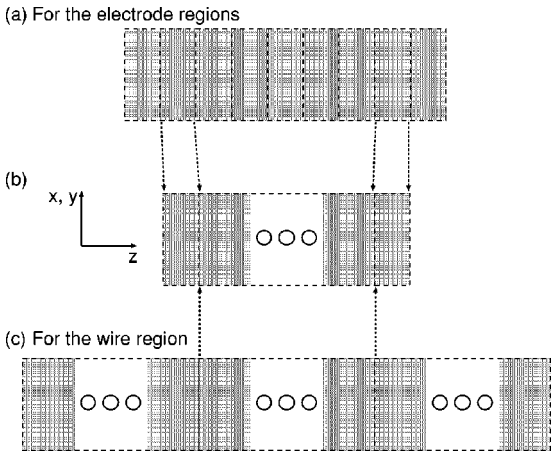

FIG. 1. Supercell model used for the self-consistent potential calculation in (a) the electrode and (c) the wire regions. (b) The potential of an atomic wire between two semi-infinite electrodes consists of the potentials generated for each region. Note that the cells are also periodic in the direction perpendicular to the wire.

The self-consistent potentials in the three regions are smoothly connected and constitute the potential $V(\boldsymbol{r})$ for an injected electron [Fig. 1(b)]. The wave function Ψ_k for each electron with a certain incident energy E is written as

$$\Psi_k = \begin{cases} \psi_k + \sum_{k' \in L} r_{k'k}\psi_{k'} & \text{(in left electrode region)}, \\ \sum_n a_n \psi_n & \text{(in wire region)}, \\ \sum_{k' \in R} t_{k'k}\psi_{k'} & \text{(in right electrode region)}, \end{cases} \tag{1}$$

where L (R) represents the states moving leftward (rightward), and the ψ_n's are linearly independent solutions of the Kohn-Sham equation. The coefficients $r_{k'k}, a_n$, and $t_{k'k}$ are determined by the boundary condition that the wave function and its derivative are continuous at the region boundaries. In each region of Eq. (1), the WFM method [18] is used to solve the Kohn-Sham equation, as is explained below.

In the xy plane we still use the large periodic cell to simulate an isolated wire connected to electrodes. The wave functions and the self-consistent potential are then Fourier transformed by introducing two-dimensional reciprocal vectors $\boldsymbol{G}_\perp$. The number of $\boldsymbol{G}_\perp$ is taken so as to be consistent with the plane-wave cutoff energies that are employed to calculate the self-consistent potential $V(\boldsymbol{r})$.

Along the z direction, we introduce the real-space mesh $\{z_n\}$. The mesh spacing $\delta z \equiv z_{n+1} - z_n$ should be sufficiently

small and the self-consistent potential $V(\boldsymbol{r})$ is assumed to be z independent in each slab of thickness δz: i.e., the potential $V(\boldsymbol{r})$ is discretized and regarded as a set of z-independent potentials $\{V_n(\boldsymbol{r}_\perp)\}$. We examined the convergence of the mesh spacing, and $\delta z = 0.45$ and 0.37 a.u. are found to be sufficient for Al and Si, respectively.

The Kohn-Sham equation in the three-dimensional real space is thus converted to linear equations in the $\boldsymbol{G}_\perp$ space for each slab n. Within a slab, analytic expressions for all propagating and evanescent waves are obtained and they are connected smoothly to the expressions in adjacent slabs. In the electrode region, the periodic boundary condition is applied in the z direction. As a result of this, complex band structures with possible imaginary wave numbers appear. For every propagating Bloch wave with real wave number k coming to the wire region, the wave function is calculated so as to connect the incident, reflected, and transmitted waves smoothly. We then finally obtain the transmission probability $t_{k'k}$ from the computed wave function (1).

Finally, the conductance is calculated by the multichannel Landauer formula. For an incident electron with energy E, the conductance $G(E)$ is written as

$$G(E) = G_0 \mathrm{Tr}[\mathbf{t}(E)^\dagger \mathbf{t}(E)], \tag{2}$$

where $\mathbf{t}(E) \equiv \{t_{k'k}\}$ is the transmission matrix. In the experiments, $G(E)$ at the Fermi energy E_F is measured when the bias voltage is close to zero. It is shown that there is a unitary transformation U which diagonalizes the matrix $\mathbf{t}^\dagger\mathbf{t}$: i.e., $\mathrm{U}^\dagger\mathbf{t}^\dagger\mathbf{t}\mathrm{U} = \mathrm{diag}\{\tau_i\}$, where $\mathrm{diag}\{\tau_i\}$ is the diagonal matrix. Then Eq. (2) becomes

$$G(E) = G_0 \sum_i^N \tau_i(E). \tag{3}$$

Thus $\tau_i(E)$ is the transmission probability of each channel $i(=1, \ldots, N)$, and the channel is regarded as an eigenchannel.

III. RESULTS AND DISCUSSION

A. Single-line wires

We first study the conductance of Al and Si wires consisting of a single line of atoms. The number of atoms in a wire ranges from one to eight in this paper. For the interatomic distance in the wires we adopt 5.4 a.u. for Al wires and 4.4 a.u for Si wires. The values are the corresponding distances in bulk fcc Al and diamond-structured Si, respectively.

1. Conductance $G(E)$

We first present the conductance at the Fermi energy $G(E_F)$ as a function of the wire length (Fig. 2). The conductance depends on the wire length for both the Al and Si wires. Both the wires take the maximum value of almost 3.0 G_0 in the five-atom wire. Yet the variation of the conductance is rather different for the two elements. In Al, $G(E_F)$ varies by $(0.2\text{–}0.6)G_0$ when the number of atoms increases by one. On the other hand, the corresponding change for Si wires is $(0.01\text{–}0.2)G_0$. The conductance of the Si wires is less sensitive to the length of the wires. The origin of this behavior is discussed later in terms of the electron states of the wires.

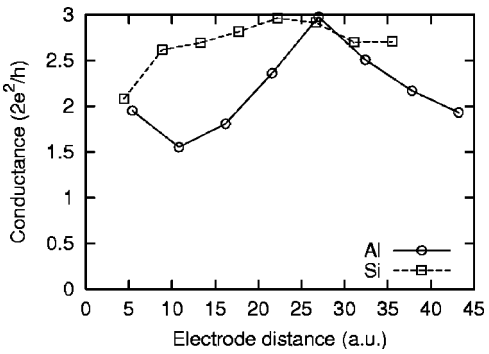

FIG. 2. The conductance at the Fermi energy $G(E_F)$ of Al and Si single-line straight wires consisting of one to eight atoms. The abscissa, the distance between the left and right electrodes, is a measure of the length of the wire consisting of one to eight atoms.

It is interesting to see the conductance $G(E)$ for an incident electron with different energy. Figure 3 shows the conductance $G(E)$ as a function of the incident electron energy E for two Al wires consisting of three and five atoms. Below $E = -6$ eV the conductance is negligible for both wires. The conductance increases rapidly around $E = -6$ eV and saturates to $G = 1G_0$ with a slight oscillation. This oscillatory behavior of the conductance is enhanced for longer wires, as is shown in Fig. 3, and is interpreted in terms of the commensurability between the electron wavelength and the electrode distance.[10,25] The conductance is unity until E reaches E_F and then increases to $3G_0$. Again, the conductance oscillates around $G = 3G_0$ until E reaches 3 eV. Then $G(E)$ increases monotonically.

$G(E)$ of the three- and five-atom Si wires is shown in Fig. 4. The conductance is negligible below $E = -10$ eV and then becomes almost constant with the value of $G = 1G_0$ from $E = -10$ to -2 eV. Then it increases to $3G_0$ when $E = -2$ to 3 eV. In contrast to the Al wires, there is a dip in the conductance around $E = -2$ eV.[26] The dip for the five-atom wire is larger than that for the three-atom wire.

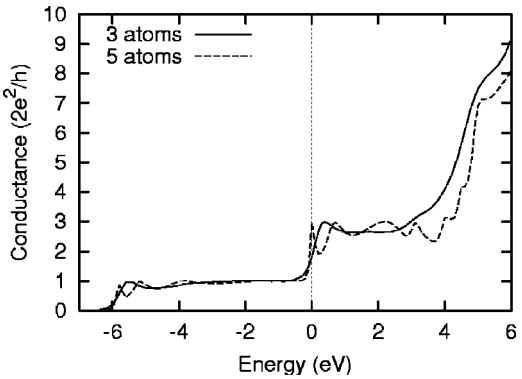

FIG. 3. The conductance of three- and five-atom single-line straight Al wires as a function of incident electron energy. The Fermi energy E_F is at $E = 0$.

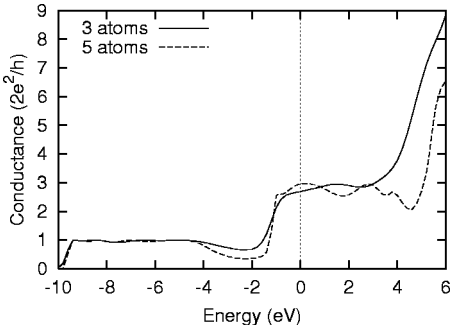

FIG. 4. The conductance of three- and five-atom single-line straight Si wires as a function of incident electron energy.

2. Eigenchannel analysis of $G(E)$

Because $G(E)$ reflects the total transmission, which is the sum of contributions from all channels, the physical origin of the conductance and its detailed features still remain unclear. We thus performed eigenchannel analysis of the conductance for each incident energy and then clarified the relation between the eigenchannels and the electron states of infinite-length wires.

Figure 5 shows the transmission probability $\tau_i(E)$ for each eigenchannel i of (a) three-atom and (b) five-atom Al wires as a function of the incident energy E. The first channel opens at $E=-6$ eV. The second and third channels are degenerate and open just below the Fermi energy. The transmission probabilities of these channels rapidly saturate to $\tau_i \sim 1$ and oscillate after they open. Thus the number of channels open at the Fermi energy is three.

Opening of the eigenchannels is closely related to the electron states of the infinite-length wire shown in Fig. 5(c): The energy at which the first channel starts to open corresponds to the bottom of the σ band. The σ band consists of s and p_z orbitals of Al. On the other hand, the energy at which the second and third channels open corresponds to the bottom of the π bands consisting of the p_x and p_y orbitals.

These correspondences are visible in Fig. 6 where the eigenchannel wave functions at E_F are shown. The eigenchannel wave functions ϕ_i are obtained by unitary transformation of the wave functions (1) by using the unitary matrix $U=(u_{ki})$, which diagonalizes the product of the transmission matrices $\mathbf{t}^\dagger\mathbf{t}$:[13]

$$\phi_i = \sum_k u_{ki}\Psi_k . \tag{4}$$

It is clear that the three open channels at E_F have the characters of σ and π states, respectively.

The same analyses were done for the Si wires. Figure 7 is the eigenchannel transmission probability of (a) three- and (b) five-atom Si wires. The energy bands of the infinite-length Si wire are also shown in Fig. 7(c). There are three open channels at E_F. The first channel, which has σ character, starts to open at $E=-10$ eV. In contrast to the Al wires, this has a dip in transmission around $E=-2$ eV. The second and third channels, which have π character, are degenerate and open at $E=-2$ eV. The energy where the dip appears corresponds to the energy gap of the σ band of the infinite-length wire as seen in Fig. 7(c). It is noteworthy that a gap in the energy band causes a transmission dip only in the corresponding channel: The first channel of the Si wire has a dip around $E=-2$ eV, whereas the second and third channels are unaffected.

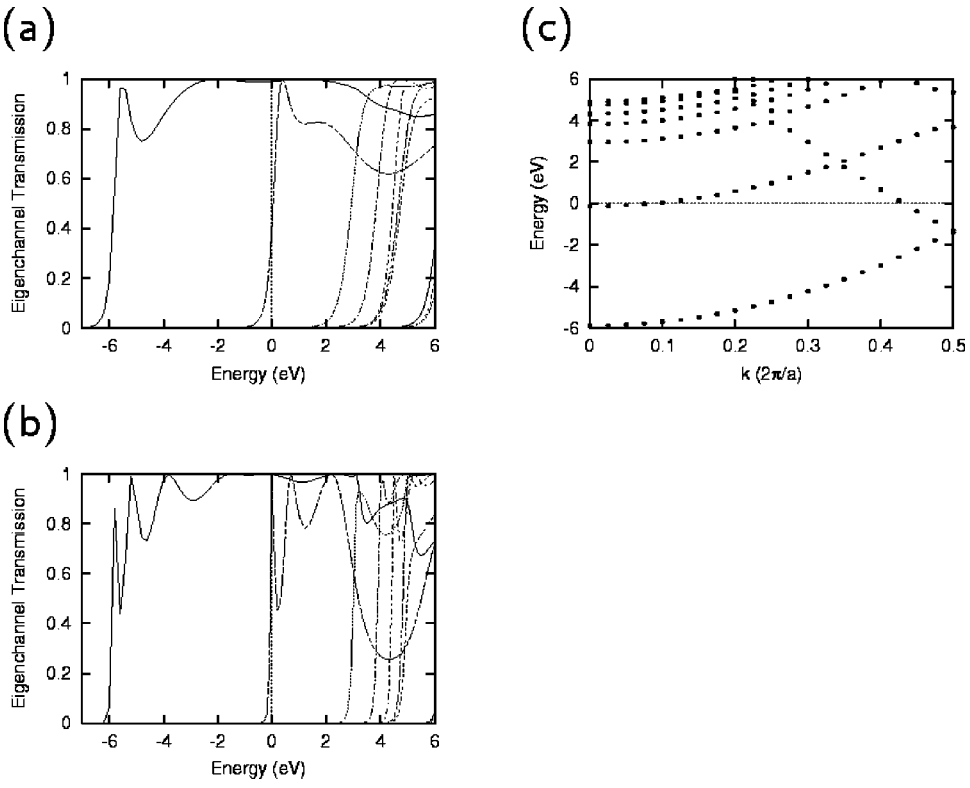

FIG. 5. The eigenchannel transmission of the (a) three- and (b) five-atom Al wires. Each line represents τ_i in Eq. (3) as a function of the incident energy. (c) The energy-band structure of the infinite-length Al wire. The Fermi energy is at $E=0$.

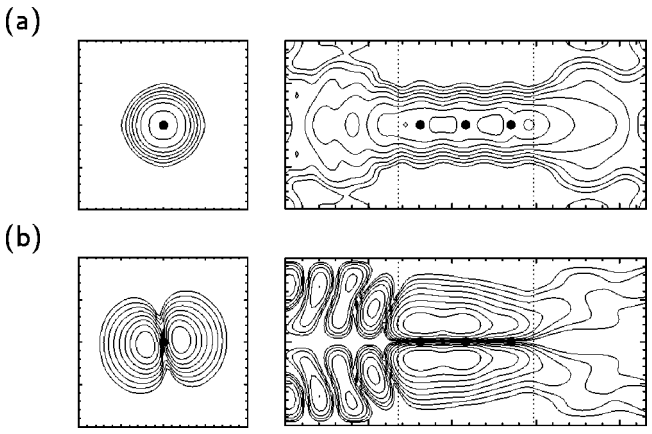

FIG. 6. Contour plots of the squared eigenchannel wave functions of a three-atom Al wire at the Fermi energy. (a) first and (b) second (third) channels. The left panel is in the xy plane cutting the center atom. The right panel is in the plane that contains the wire. The electron is incident from the left. Black circles indicate the atomic positions. Vertical dotted lines are the edges of the jellium electrodes.

We are now in position to discuss the origin of the conductance behaviors of the Al and Si wires. The number of open channels is three at the Fermi energy for both wires. This sets the upper bound of the conductance, leading to the maximum conductance $3G_0$.

The dip in $G(E)$ of the Si wire below E_F (Fig. 4) originates from a dip in the first channel in Figs. 7(a) and 7(b). The width of the dip becomes narrower as the length of the wire increases, because the period of the resonant peaks gets shorter for a longer wire. For the three-atom Si wire the dip around $E=-2$ eV crosses E_F, whereas the dip in the five-atom Si wire is narrower and the transmission recovers to $\tau_i=1$ at E_F. On the other hand, the second and third channels are almost fully open at E_F for all wire lengths. Consequently, only the first channel is responsible for the variation of the conductance as the wire length changes.

On the other hand, the first channel in the Al wire is fully open at E_F irrespective of the wire length, and the other two are partially open. For a longer wire, the slope of the transmission probability is steeper due to less contribution of the evanescent waves. Also, oscillatory behaviors are enhanced owing to the increasing number of electron wavelengths that satisfy the commensurability condition with the wire length. Hence the transmission probability of the channel which opens at E_F is sensitive to structural changes such as the wire length. In addition, the two degenerate (second and third) channels contribute to the conductance change. Therefore a maximum variation of $\sim 2G_0$ could be possible. That is why the conductance of the Al wire varies more than that of the Si wire with changing wire length.

Correlation between the conductance and the electron states is generally expected. Actually, Mozos *et al.*[26] calculated the conductance of Si wires, found the conductance dip below E_F, and interpreted it in terms of a gap in the band structure of the infinite-length wire. As is clear in Fig. 7, however, the calculated transmission probabilities for eigenchannels are sensitive to the incident energy and to the structural variation of finite-length wires. The transmission probabilities of eigenchannels are the eigenvalues of the product of the transmission matrices $\mathbf{t}^{\dagger}\mathbf{t}$. Among the eigenvalues, most of them have negligible values except for a few open channels. Hence, only after eigenchannel decomposition can

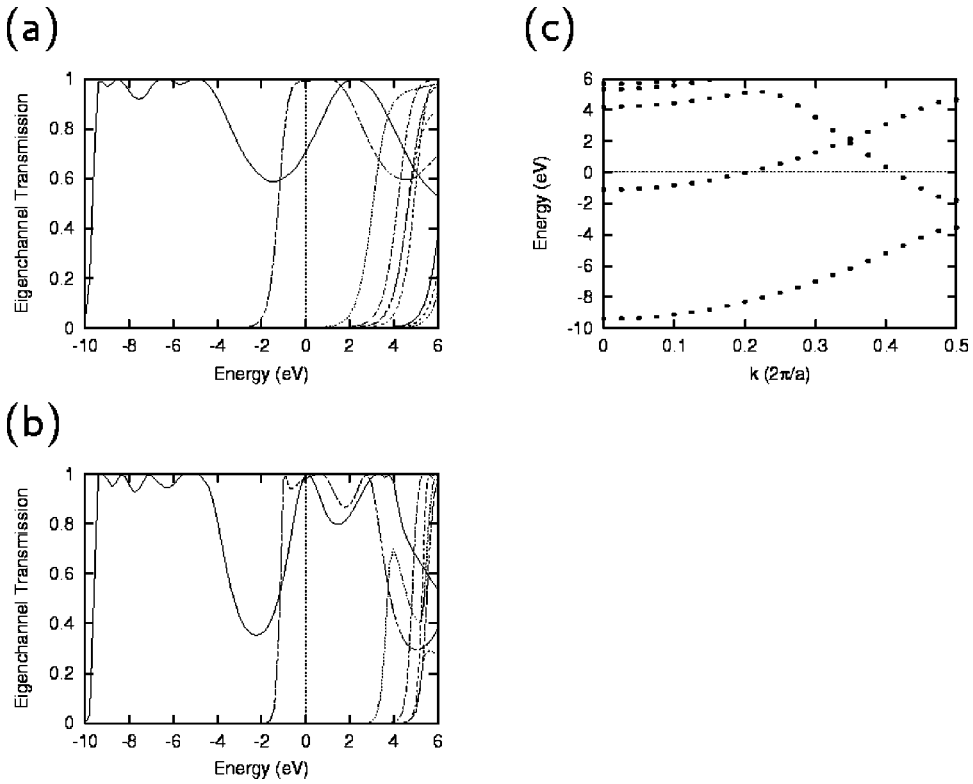

FIG. 7. The eigenchannel transmission of the (a) three- and (b) five-atom Si wires. Each line represents τ_i in Eq. (3) as a function of the incident energy. (c) The energy-band structure of the infinite-length Si wire. The Fermi energy is at $E=0$.

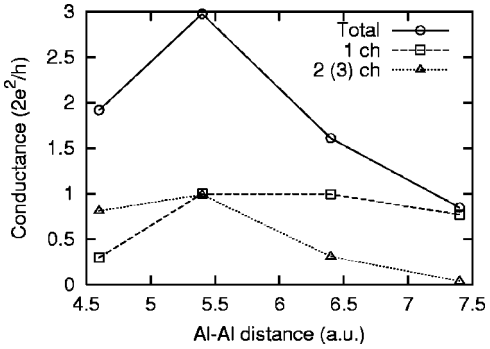

FIG. 8. The conductance and the eigenchannel transmission of a five-atom single-line Al wire at the Fermi energy as a function of the Al-Al distance. The solid line with circles, the dashed line with squares, and the dotted line with triangles denote the total conductance, and the first and second (the third) eigenchannel transmission probabilities, respectively. The second and third channels are degenerate.

the correspondence between the states in the bands and the open channels in the wires be clarified.

B. Effects of stretching wires

As discussed in the previous subsection, the eigenchannel transmission of a finite-length atomic wire between jellium electrodes is closely related to the band structure of an infinite-length wire. We therefore expect that structural deformations of the wire induce changes in the electron states, lead to variations in the eigenchannel transmission, and eventually cause variations in the conductance. It is thus useful to know the electron states of an infinite-length wire for predicting the conductance and its change upon deformation. In this subsection, we elucidate generic features of Al nanowires and then discuss the observed increase[5,7] in the conductance upon stretching.

We focus on the conductance of the five-atom single-line Al wire. In the previous subsection we set the Al-Al distance d in the wire to be 5.4 a.u. We now change it in the range of $d=4.6$–7.4 a.u. for comparison. The value 4.6 a.u. is the optimized geometry for an infinite-length single-line Al wire.[27]

Figure 8 shows the conductance and the eigenchannel transmission at the Fermi energy as a function of the Al-Al distance. The conductance of the shortest wire ($d=4.6$ a.u.) is $1.9G_0$, which is substantially smaller than the value $3.0G_0$ for the stretched wire ($d=5.4$ a.u.) discussed in the previous subsection. Stretching the Al-Al distance ($d>5.4$ a.u.) decreases the conductance. The transmission probabilities of the three channels increase when the Al-Al distance is stretched from 4.6 a.u. Upon further stretching ($d>5.4$ a.u.), the second and third channels close more rapidly than the first channel.

In Fig. 9, the eigenchannel transmission of the shortest wire and the energy-band structure of the corresponding infinite-length wire are shown. The number of open channels is found to be three at E_F. The decrease in the conductance of the shortest wire that we have found is caused mainly by

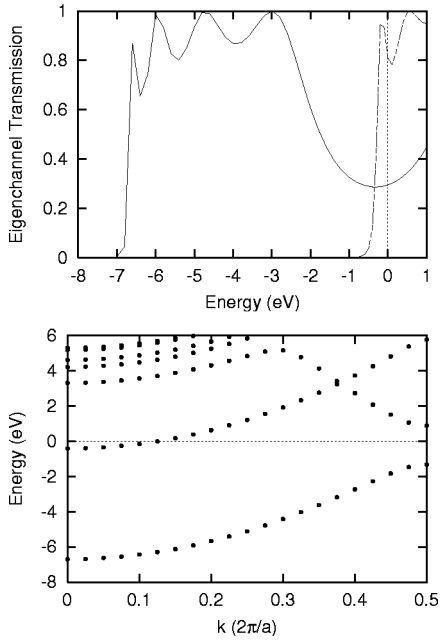

FIG. 9. The eigenchannel transmission and the energy-band structure of an Al wire with a shorter bond length 4.6 a.u.

the dip in transmission of the first channel. The first channel corresponds to the σ band, which has an energy gap around E_F. Thus the transmission of the first eigenchannel decreases to $\tau_1 \sim 0.3$. On the other hand, it is found that the transmission probabilities of the second and third channels are $\tau_2, \tau_3 \sim 0.8$. This amounts to the total conductance of $1.9G_0$.

The increase in the conductance upon stretching, or more generally the change in the conductance upon deformation of wires, is explained naturally by the combination of the changes of the energy-band structure of an infinite-length wire and the corresponding eigenchannel transmission probabilities.

In order to further explain this point, let us consider the band structures of infinite-length single-line wires with one s and three p orbitals (Fig. 10). When atoms come together, the s and p_z orbitals in isolated atoms constitute corresponding "s" and "p_z" bands[30] or mix substantially and form σ bands, whereas the p_x and p_y orbitals constitute corresponding π bands. For a large Al-Al distance, overlaps of the adjacent orbitals and thus the band widths are small. When the widths of the "s" and "p_z" bands are small compared with the difference between the s and p_z levels, the "s" and "p_z" bands do not cross. Consequently, there is a gap between the top of the "s" band and the bottom of the "p_z" band [Fig. 10(a)]. As the bond length decreases, the overlaps of the orbitals become larger so that the bandwidths increase. At a certain distance, the top of the "s" band and the bottom of the "p_z" band touch and the gap disappears [Fig. 10(b)]. When the bond length decreases further, the "s" and "p_z" bands could cross as shown by the dashed lines in Fig. 10(c) in the absence of the mixing. Yet actually with the s-p_z mixing the bands repel each other. Therefore a gap reappears between the "s" and "p_z" bands, as shown by the solid lines in Fig. 10(c).

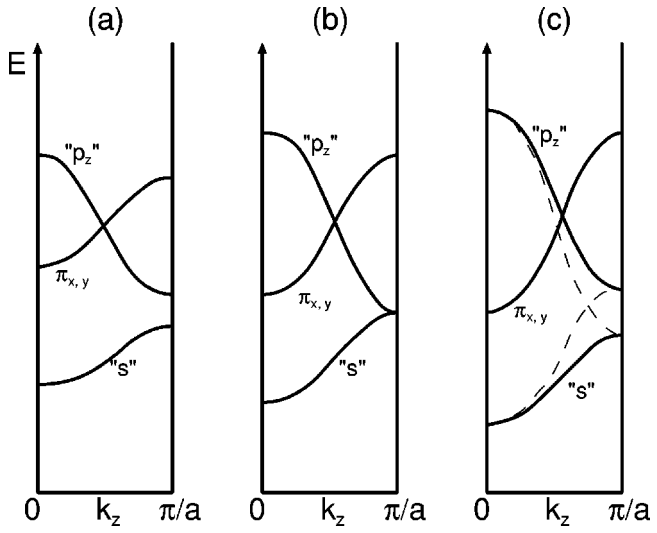

FIG. 10. Schematic illustration of the energy bands of an infinite-length single-line wire with different bond lengths. The bond length decreases from (a) to (c).

Based on the band structure discussed above, the effects of wire stretching on the conductance become clear. For Al there are three electrons per atom so that the first σ band is completely filled. The $\pi_{x,y}$ and "p_z" bands are partially filled. Although the occupation changes depending on the relative positions of the *s* and *p* levels and the bandwidth, the Fermi energy will be located somewhere in these $\pi_{x,y}$ bands. For the smaller Al-Al distance in (c), the band is similar to that for the distance 4.6 a.u. shown in Fig. 9. The $\pi_{x,y}$ bands are partially filled and the "p_z" band is empty. The Fermi energy is located in the gap between the "s" and "p_z" bands. Thus two channels corresponding to $\pi_{x,y}$ open. Further a channel corresponding to the s-p_z band will also open, but have a dip in the transmission probability around E_F. Consequently, the conductance is not larger than $2G_0$ (from $\pi_{x,y}$ channels) plus a small contribution from the the s-p_z channel. When the wire is stretched, the band becomes like Fig. 10(b). The energy gap disappears. The Fermi energy will be located near the bottom of the $\pi_{x,y}$ band. This is the situation shown in Fig. 5(c) for the Al-Al distance of 5.4 a.u. The maximum conductance becomes $3G_0$ when all the channels open completely. For further elongation, the gap reappears and the Fermi energy comes near the bottom of the "p_z" band. In this case, the maximum conductance may be $1G_0$ when the $\pi_{x,y}$ bands are both empty.

Thus the conductance will increase from (c) to (b), and then decrease from (b) to (a) upon stretching. It will be possible to increase or decrease the conductance just by stretching. Stretching a wire with the shorter bond length increases the conductance, whereas the conductance decreases upon stretching the wire with a moderate bond length.

One of the striking features of the conductance of Al point contacts is the positive slope during stretching. Based on their tight-binding calculations, Cuevas *et al.*[6] argue that the stretching makes the Fermi energy lie at the peak of the local density of states and thus increases the conductance. On the other hand, based on a DFT calculation, Kobayashi *et al.*

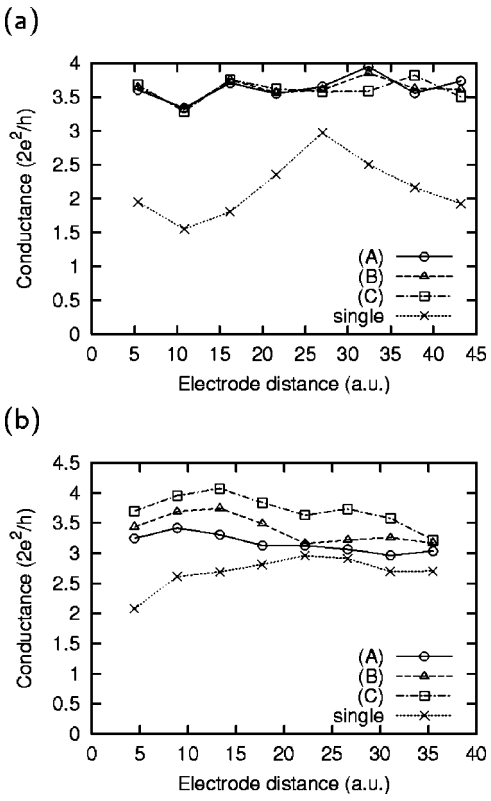

FIG. 11. The conductance of double-line wires with different interline separations at E_F. The number of atoms in each wire ranges from one to eight. (a) For Al the separations *s* are (A) 5.0, (B) 5.4, and (C) 6.0 a.u., respectively, and (b) for Si, they are (A) 4.0, (B) 4.4, and (C) 5.0 a.u., respectively. The conductance of the single-line wire is also shown for comparison.

propose that the increase in the conductance is due to straightening a bent wire during elongation.[13] Our calculations along with the qualitative discussion above clarify that the reason for the positive slope of the Al contact is the bond stretching. The discrepancy in the conductance variation during the bond stretching between ours and the other DFT calculation in Ref. 13 can be understood by the difference of the initial bond length. In Ref. 13 the authors began with the bond length 5.4 a.u., stretched the bond, and found a decrease in the conductance. This corresponds to the change from (b) to (a) in Fig. 10. On the other hand, we stretched the bond from the shorter length 4.6 a.u. to 5.4 a.u., and found an increase in conductance, which corresponds to the change from (c) to (b). Both of the two DFT results are naturally explained by our qualitative analyses above.

C. Double-line wires

We next explore nanowires consisting of two straight atomic lines parallel to each other. Each atomic line is identical to the single atomic line with *n* atoms discussed in Sec. III A. The interatomic distance in the wires and the jellium-wire distance are the same as before. A new degree of freedom, i.e., the separation *s* between the two parallel lines, is introduced in these atomic wires. We try to elucidate the effects of the separation on the conductance. Three kinds of

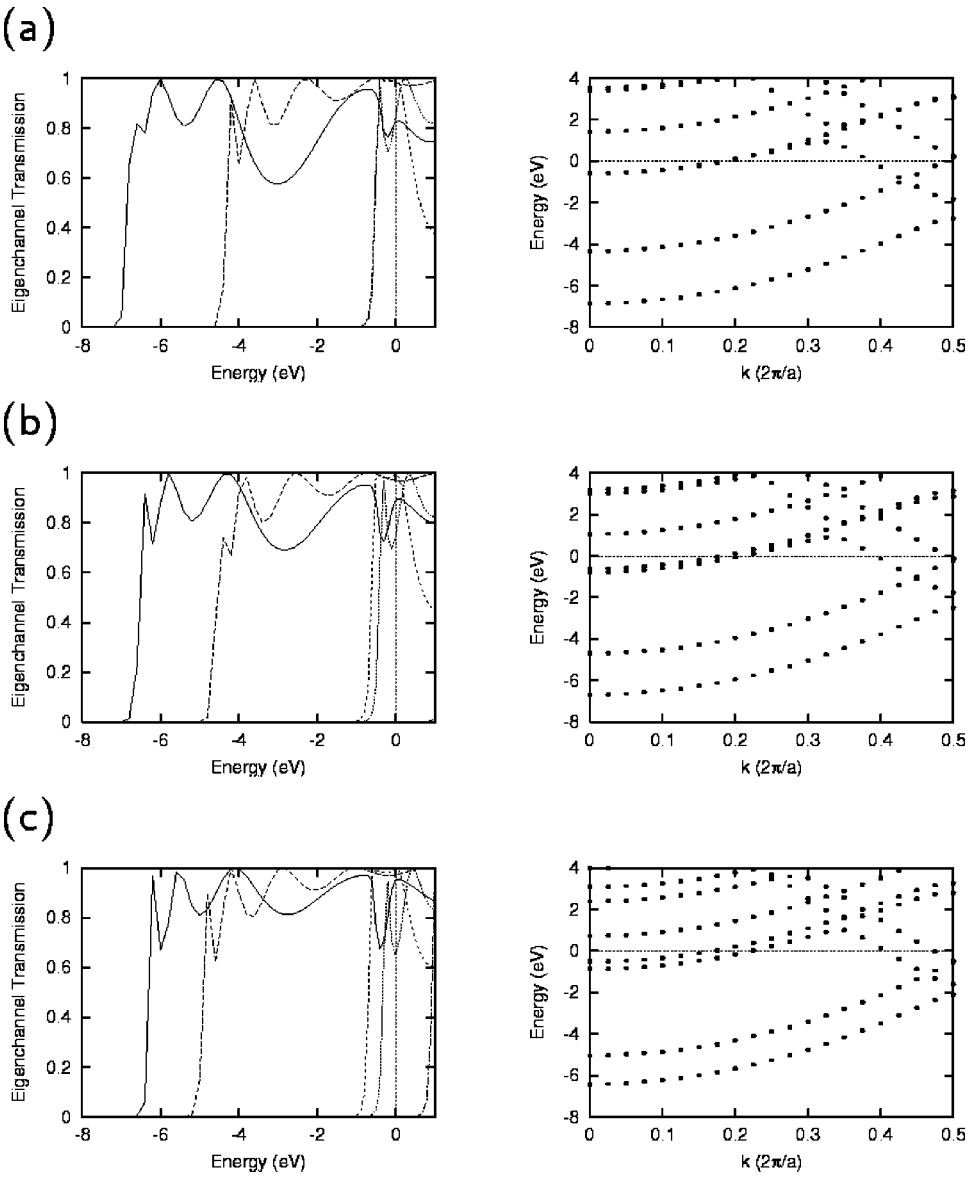

FIG. 12. The eigenchannel transmission of double-line five-atom-length Al wires and the energy-band structure of the infinite-length Al wire. The interline separation s is (a) 5.0, (b) 5.4, and (c) 6.0 a.u.

wires with different separations s are investigated. For Al wires, $s=5.0$,5.4, and 6.0 a.u., whereas in Si $s=4.0$,4.4, and 5.0 a.u.

The conductances of double-line wires consisting of atomic single lines of one to eight atoms are calculated at the Fermi energy for different separations s. They are shown in Figs. 11(a) for Al and 11(b) for Si. It is clear that the conductance of the double-line wire is not simply twice that of the single-line wire for both elements. For Al, the conductance is insensitive to the wire separation, and the dependence on the wire length is also reduced. In the case of Si, the larger the separation, the larger is the conductance for all wire lengths. A small dependence on the wire length is observed as for the single-line wires.

Figure 12 shows the eigenchannel transmission of double-line five-atom-length Al wires and the band structure of the infinite-length Al wire for three separations. For Al wires, the number of open channels is four at the Fermi energy. There is no energy gap around the Fermi energy, which is located far from the band edges. Therefore the eigenchannels have no dips so that the transmission probabilities of these channels are high. Although the onset energies of the channel opening are slightly shifted by changes of the interactions between the atomic lines, the band structure of the Al wires around the Fermi energy is not drastically changed. Thus the conductance is relatively robust to variation of the interline separation.

The eigenchannel transmission of double-line five-atom-length Si wires, along with the energy bands of the infinite-length wire with three separations, are presented in Fig. 13. We have found that five channels are open at E_F. Among the five open channels of the Si wires, three of them have a dip across the Fermi energy. The channels with these dips correspond to energy gaps near or around the Fermi energy. Changing the interline separation alters the band structure, and consequently the positions of the dips shift relative to the Fermi energy. As a result, the total transmission of each channel is affected by widening the separation. Since even a slight shift results in a large variation of the transmission

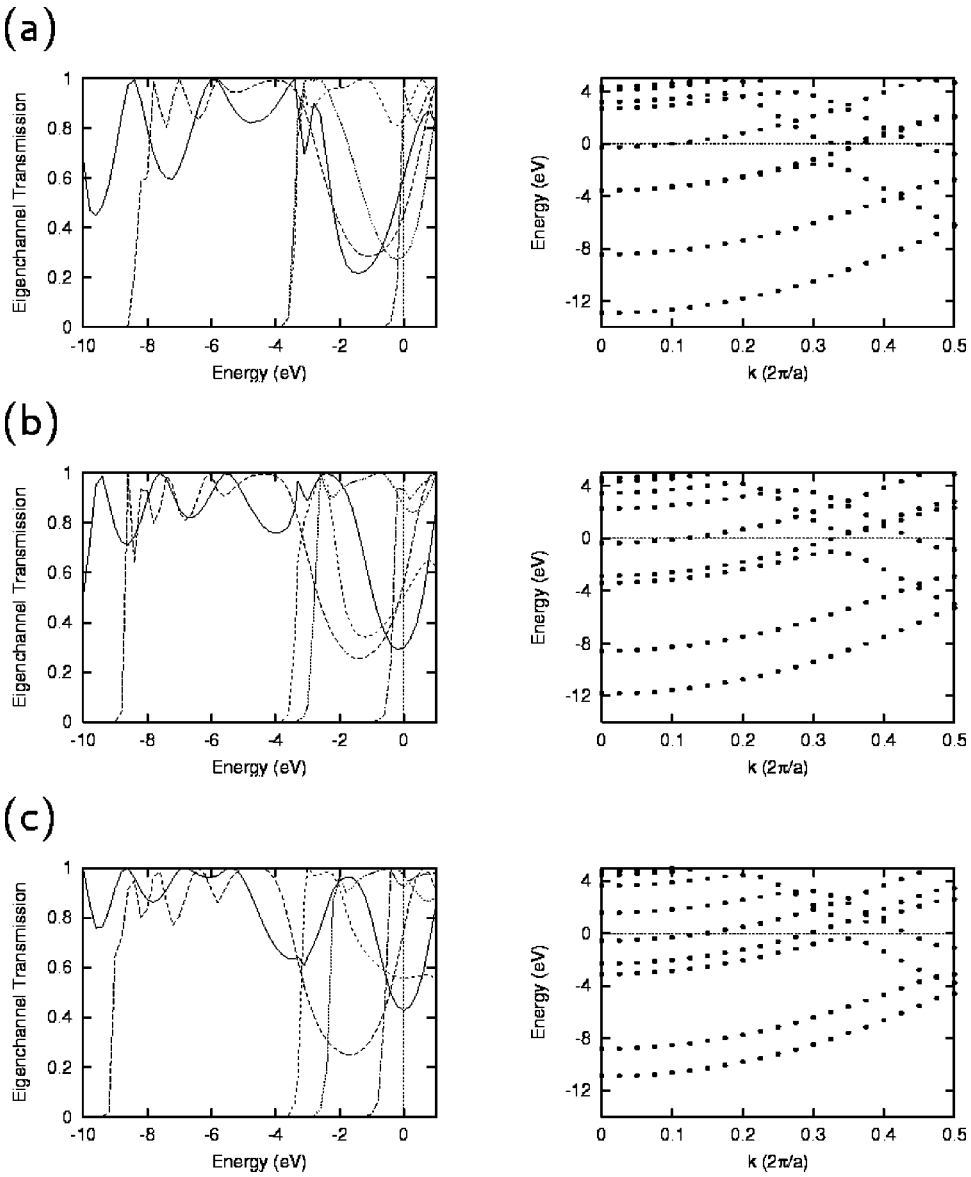

FIG. 13. The eigenchannel transmission of double-line five-atom-length Si wires and the energy-band structure of the infinite-length Si wire. The interline separations are (a) 4.0, (b) 4.4, and (c) 5.0 a.u., respectively.

probability around the dips, the conductance of the double-line Si wires depends sensitively on the interline separation.

For the Si wires, we also note that the number of bands crossing the Fermi energy is three, whereas the number of open channels is five. The three channels for the bands crossing the Fermi energy and the two channels corresponding to the energy gap make five open channels. The number of open channels is sometimes evaluated only from the number of bands crossing the Fermi energy.[27–29] As is demonstrated here, however, it is necessary to include small but finite contributions from the channels which correspond to electron states off the Fermi energy in order to obtain accurate prediction of the number of open channels, especially for short wires.

IV. CONCLUSION

We performed first-principles calculations of the conductance of Al and Si atomic wires between jellium electrodes using the wave-function matching method combined with the density functional theory.

We found that the conductance varies with changing wire length and takes its maximum value of $3G_0$ at some finite length for single-line Al or Si atom wires. Variation of the conductance as a function of the wire length is substantially different for the two elements adjacent to each other in the periodic table: The Al wires show larger variations upon addition of a single atom than do the Si wires. The origin of the similarity and dissimilarity between the Al and Si wires has been unequivocally clarified by our eigenchannel analysis.

We have also investigated the conductance of double-line Al and Si wires and found that the chemical difference makes the conductance of atom wires richer: The conductance of the double-line Al wires has little dependence on the separation between single atom lines, whereas the conductance of the double-line Si wires exhibits substantial variation with changing separation; the numbers of open channels in the Al and Si double-line wires are different from each

other. We found that this interesting dissimilarity between Al and Si wires is well understood in terms of the energy bands of the corresponding infinite-length wires, once the eigenchannel decomposition is performed. In particular, it is found that the electron states not located at the Fermi energy contribute substantially to the eigenchannel transmission and thus the conductance.

As a remarkable example of these approaches, we clarified the origin of the conductance increase upon stretching which has been observed for Al wires: The energy bands of wires consisting of group III or IV atoms with *s* and *p* levels exhibit a peculiar dependence on the interatomic distance, which plays an essential role in the conductance. We emphasize that the eigenchannel analysis combined with quantitative quantum calculations for the wave functions of the scattering electrons is a useful tool to interpret and predict the conductance of nanowires.

ACKNOWLEDGMENTS

This work was partly supported by ACT-JST (Japan Science and Technology Corporation), Special Research Project on Nanoscience at the University of Tsukuba, NEDO under the Nanotechnology Materials Program, the NEDO Collaboration Program, and a Grant-in-Aid for Scientific Research from the Ministry of Education, Science, and Culture of Japan. Computations were done at the Institute for Solid State Physics, University of Tokyo, at the Science Information Processing Center, University of Tsukuba, and at the Research Center of the Computational Science, Okazaki National Institute.

[1] N. Agraït, A. Levy Yeyati, and J. M. van Ruitenbeek, Phys. Rep. **377**, 81 (2003).
[2] H. Ohnishi, Y. Kondo, and K. Takayanagi, Nature (London) **395**, 780 (1998).
[3] J. M. Krans, C. J. Muller, I. K. Yanson, T. C. M. Govaert, R. Hesper, and J. M. van Ruitenbeek, Phys. Rev. B **48**, 14 721 (1993).
[4] D. Sánchez-Portal, C. Untiedt, J. M. Soler, J. J. Sáenz, and N. Agraït, Phys. Rev. Lett. **79**, 4198 (1997).
[5] E. Scheer, P. Joyez, D. Esteve, C. Urbina, and M. H. Devoret, Phys. Rev. Lett. **78**, 3535 (1997).
[6] J. C. Cuevas, A. Levy Yeyati, A. Martín-Rodero, G. R. Bollinger, C. Untiedt, and N. Agraït, Phys. Rev. Lett. **81**, 2990 (1998).
[7] E. Scheer, N. Agraït, J. C. Cuevas, A. Levy Yeyati, B. Ludoph, A. Martín-Rodero, G. R. Bollinger, J. M. van Ruitenbeek, and C. Urbina, Nature (London) **394**, 154 (1998).
[8] N. D. Lang, Phys. Rev. B **52**, 5335 (1995).
[9] N. Kobayashi, M. Brandbyge, and M. Tsukada, Jpn. J. Appl. Phys., Part 1 **38**, 336 (1999).
[10] C. C. Wan, J.-L. Mozos, G. Taraschi, J. Wang, and H. Guo, Appl. Phys. Lett. **71**, 419 (1997).
[11] J. J. Palacios, A. J. Pérez-Jiménez, E. Louis, E. SanFabián, and J. A. Vergés, Phys. Rev. B **66**, 035322 (2002).
[12] M. Brandbyge, M. R. Sørensen, and K. W. Jacobsen, Phys. Rev. B **56**, 14 956 (1997).
[13] N. Kobayashi, M. Brandbyge, and M. Tsukada, Phys. Rev. B **62**, 8430 (2000).
[14] N. Kobayashi, M. Brandbyge, and M. Tsukada, Surf. Sci. **433–435**, 854 (1999).
[15] P. Hohenberg and W. Kohn, Phys. Rev. **136**, B864 (1964).
[16] W. Kohn and L. J. Sham, Phys. Rev. **140**, A1133 (1965).
[17] M. Büttiker, Y. Imry, R. Landauer, and S. Pinhas, Phys. Rev. B **31**, 6207 (1985).
[18] H. J. Choi and J. Ihm, Phys. Rev. B **59**, 2267 (1999).
[19] W. E. Pickett, S. G. Louie, and M. L. Cohen, Phys. Rev. B **17**, 815 (1978).
[20] M. Schlüter, J. R. Chelikowsky, S. G. Louie, and M. L. Cohen, Phys. Rev. B **12**, 4200 (1975).
[21] D. M. Ceperley and B. J. Alder, Phys. Rev. Lett. **45**, 566 (1980).
[22] J. P. Perdew and A. Zunger, Phys. Rev. B **23**, 5048 (1981).
[23] N. D. Lang, Phys. Rev. B **49**, 2067 (1994).
[24] N. D. Lang and A. R. Williams, Phys. Rev. B **18**, 616 (1978).
[25] E. Tekman and S. Ciraci, Phys. Rev. B **39**, 8772 (1989).
[26] J.-L. Mozos, C. C. Wan, G. Taraschi, J. Wang, and H. Guo, Phys. Rev. B **56**, R4351 (1997).
[27] P. Sen, S. Ciraci, A. Buldum, and I. P. Batra, Phys. Rev. B **64**, 195420 (2001).
[28] I. P. Batra, P. Sen, and S. Ciraci, J. Vac. Sci. Technol. B **20**, 812 (2002).
[29] F. D. Tolla, A. D. Corso, J. A. Torres, and E. Tosatti, Surf. Sci. **454–456**, 947 (2000).
[30] We label the bands by symbols with double quotation marks, for they are formed by mixing the atomic *s* and p_z orbitals.